World Journal of Pharmaceutical Sciences
ISSN (Print): 2321-3310; ISSN (Online): 2321-3086
Published by Atom and Cell Publishers
Available online at: http://www.wjpsonline.org/
Original Article

Preparation and characterization of L – Dopa loaded chitosan – based dry powder: Rescue / continuous supplement in Parkinson's disease via inhalation

A.A. Yas, Department of Pharmaceutics, College of Pharmacy, Tikrit University, Tikrit–P. O. Box [42], Saladin–Iraq

Received: 04-12-2015 / Revised: 21-12-2015 / Accepted: 28-12-2015 / Published: 01-01-2016

ABSTRACT

L – Dopa (LD) oral administration for controlling Parkinson's disease (PD) motor symptoms at the later stage will become inefficient pharmacodynamically due to the motor deteriorations result from LD fluctuated pharmacokinetic parameters especially gastrointestinal absorption and short plasma half-life. The goal from this work was preparing LD loaded chitosan-based dry powder nanoparticles (LD-CSNPs) for pulmonary delivery and hence reducing the dose required and frequency of administration. By employing Box-Behnken experimental design (BBD) for optimizing the dependent variables that include; the particle size (PS) [Y_1] and encapsulation efficiency (EE) [Y_2] of LD NPs prepared from chitosan (CS) by ionotropic gelation method, at different combinations of independent variables that include; CS concentration [X_1], chitosan/tripolyphosphate (CS/TPP) mass ratio [X_2] and LD/CS mass ratio [X_3]. Ultracentrifuge, dynamic light scattering and spectrophotometer were used to measure NPs EE, size and LD quantification respectively. The optimum conditions were determined by subsequent regression and multicriteria decision analyses of the output data. The independent variables had interactive effects and greatly affect both responses. The optimum conditions for NPs production are the CS concentration [X_1] of 1.2-1.6 mg/ml, CS/TPP mass ratio [X_2] of 6-7 and LD/CS mass ratio [X_3] of 1.8-2, which yielded NPs with PS range between 243-266 nm and EE% range between 53-58%. The x-ray powder diffraction (XRPD) shows that LD low intense peak reveal it's dispersion in a homogenous pattern and hence its nature becomes amorphous within the carrier and the Fourier transform infrared (FTIR) spectra shows that no physicochemical interaction occurs between the LD and the carrier. Korsmeyer-Peppas model was the best to fit the in vitro release data, the non-Fickian (anomalous) diffusion was the mechanism of release and the Weibull 4 model was the best for dissolution data fitting where the curve of release was parabolic (b<1, case 3). This procedure has optimized the LD-CSNPs PS and EE.

Keywords: Parkinson's disease, L – Dopa, Dry powder inhalation, Box – Behnken design, Cross – linked chitosan nanoparticles

INTRODUCTION

Parkinson's disease (PD) is a cureless neurodegenerative debilitating disease and the patients age more than 50 years old count in a study on the most populous nations proposed that it will be doubled from around 4.5 million in 2005 to around 9 million by 2030 [1]. For long time PD was define by Parkinsonism classical motor symptoms (includes four cardinal features: bradykinesia, rest tremor, rigidity, and postural and gait impairment) associated with Lewy bodies and substantia nigra dopaminergic neurons loss. Recently PD is considered heterogeneous with clinically significant non-motor symptoms (includes: neuropsychiatric features, dysautonomia, sleep disorders, sensory dysfunction, pain and fatigue) due to genetic and environmental factors affecting cellular processes [2]. Dopamine precursor, L-dopa (LD) administration initiation is an essential milestone necessity for improving PD patients' life quality especially controlling motor symptoms through gaining back neurotransmission by restoring DA level within the substantia nigra still living dopaminergic neurons. Intravenous infusion was the pioneer route for LD administration, then orally but with no dopa-decarboxylase inhibitor (DDI) in combine. Benserazide (BE) and Carbidopa (CD) do not cross blood-brain barrier, as DDI aid in the reduction of peripheral degradation of LD to dopamine, prolong LD plasma half-life and four-five folds reduction in oral dose, hence peripheral side effects, such as nausea and vomiting, ameliorate [3].

Since 1960s, LD stills the gold standard for treating PD symptoms and in comparison with DA

Corresponding Author Address: Dr. ALI AHMED YAS AL – JIPOURI[AA Yas**], PhD Pharmaceutics [Pulmonary Drug Delivery], Department of Pharmaceutics, College of Pharmacy, Tikrit University, Tikrit - P. O. Box [42], Saladin, Iraq; Email: dryasbiopharm@gmail.com*

agonists; LD is well tolerated as an initial monotherapy and will postpone the supplementary treatment needs. Motor deteriorations associated with prolonged LD intake (includes: wearing-off, on-off, dyskinesias and dystonias) will influence patients' life quality especially their reoccurrence prior to LD next scheduled dose. Pharmacodynamically there are LD delayed-on and no-on features; where the former is a long gap between LD intake and the appearance of the effect, whereas the latter is a complete absence of any response after LD intake and these are due to the gastrointestinal tract (GIT) variations in LD transport and absorption. The short LD half-life of 90 minutes, results in LD plasma level fluctuations and non-physiological pulsatile DA receptors stimulation due to the striatal neurons ability to take up LD and store DA for continues release and stimulation is lost because of their number depletion. By increasing the dose and the administration frequency of LD, a reduction in the wearing-off time can be attained, an approach does not pass without drawbacks; one of the major is dyskinesias (hyperkinetic involuntary movements) which can be alleviated through reducing LD dose and hence aggravates the Parkinsonism and wearing-off episodes [4].

The early and middle stages of PD motor symptoms can be controlled well with oral administration of LD, whereas at later stage it will become of minor efficacy due to the motor fluctuations and complications. Then by altering the oral route through developing novel drug delivery systems will facilitate LD delivery via buccal, transdermal, nasal or pulmonary route, and hence reduce the dose required, frequency of administration and side effects [5]. Pulmonary drug delivery can be considered the route of choice because of its non-invasiveness and large lungs surface area (~100 m^2). Also, dry powder inhalation (DPI) can be considered the pulmonary delivery system of choice due to the stability of the solid dosage form; its breath actuated advantage enables self-administration and the lowest cost among all. It will be considered as a rescue/continuous supplement of LD when being delivered via inhalation into the lungs deeply into the alveoli, hence two times less oral dose required and in comparison with oral route where peak plasma level was small and slow to reach, a rapid and higher peak plasma level achieved by DPI because of the fast drug release, fast drug absorption into the systemic circulation via the single epithelial layer lining the alveoli and finally reaching the brain avoiding GIT irregular absorption and massive metabolism [6].

The carrier being chosen for intrapulmonary LD targeting was chitosan (CS), a cationic hydrophilic polymer characterized by its biocompatibility, biodegradability, mucoadhesivness, low toxicity and role in enhancement large molecules penetrability through mucosal surfaces [7].

The following study focus on developing LD loaded CS-based dry powder nanoparticles (LD-CSNPs) utilizing a modified ionic gelation method. By implying response surface methodology (RSM) utilizing Box-Behnken experimental design (BBD) for optimization of the particle size (PS) and entrapment efficiency (EE) of LD-CSNPs, where they are properties of great influence on the pharmacokinetic (i.e.; biodistribution) and the pharmacodynamic (i.e.; therapeutic efficacy) of the drug loaded nanoparticles [8]. In comparison to the traditional experimental methods based on one variable level changing at time where the others are fixed, the experimental design provide more true data because all factors influence together will be assessed and hence optimal conditions, most influential factors and interactions exist can be determined [9]. Multicriteria decision analysis (McDA) was employed to the output data to combine PS and EE responses into a single composite response system, which is an approach that overcomes the unstructured decision-making limitations and hence enabling the selection among alternatives based on multiple criteria [10].

Furthermore, the optimized formula in vitro release profile was investigated, whereas the physicochemical characterizations include scanning electron microscopy (SEM), Fourier transform infrared spectroscopy (FTIR) and x-ray powder diffraction (XRPD) were employed for detecting particle morphology and any physicochemical interaction with the carrier.

MATERIALS AND METHODS

Materials: Pure L-dopa (LD) was received as a gift sample from the State Company for Drug Industries and Medical Appliances (SDI) (Samarra / Iraq). Chitosan (CS), acetic acid (AA) and penta-sodium triphosphate/tripolyphosphate (TPP) were produced from (Himedia-India), (Solvochime-UK) and (BDH Chemicals Ltd Poole-UK) respectively. All other chemicals/solvents used were of analytical grade.

Methodology:

Co-Polymer Preparation of L-Dopa Loaded Chitosan Nanoparticles (LD-CSNPs): Utilizing penta-sodium triphosphate (TPP) as counter ion, CSNPs were prepared by employing a modified ionotropic gelation method. According to table 1, different concentrations of CS solution were prepared in aqueous 1% v/v acetic acid under

magnetic stirring (Raypa Magnetic Stirrer AG-2/Doga Limited-Turkey) until became transparent and keep hydrating overnight. From table 1, before synthesis of NPs preweight amounts of LD were incorporated into CS solution. Then NPs instantaneously formed upon dropwise addition of prefiltered through 0.45 µm filter TPP 1 mg/ml solution into 10 ml CS solution at different CS/TPP mass ratios, table 1, under magnetic stirring at 400 rpm at room temperature and was kept stirring for 1 hour in order to assure NPs complete cross-linking. The resulting LD-CSNPs were isolated by ultracentrifugation (Universal 16A-Hettich Zentrifugen/Germany) at 20000 rpm, 10 °C and for 40 minutes. Ultrasonication (Power Sonic 410, Human Lab. Instrument Co./Korea) was employed for resuspending the precipitate in deionized water followed by freeze-drying (VirTis Freeze Dryer-Virtis Co./USA) at -55.5 °C and the EE was measured by using the supernatant [11].

LD-CSNPs Drug Entrapment Efficiency (EE %) Evaluation: The supernatant part was pulled out and free non-entrapped LD amount was spectrophotometrically determined using (SPECORD® 40- Analytik Jena AG-Germany) at 280 nm by employing the following equations [12]:

$$EE\ \% = \frac{W_t - W_s}{W_t} \times 100 \quad \text{..... (Eq. 1)}$$

where W_t is LD total amount used for NPs preparation and W_s is the free non-entrapped LD amount in the supernatant.

LD-CSNPs Particle Size Evaluation: Dynamic light scattering angle of 90 ^{0} at 25 ^{0}C was employed utilizing particle size analyzer (NanoBrook 90Plus-Brookhaven, a Nova Instruments Co./USA) to determine the particle size [13].

LD-CSNPs Optimization by RSM and McDA: A BBD was employed for the LD-CSNPs optimization utilizing 3 factors, 3 levels and 15 runs. Independent variables were coded as X_1, X_2 and X_3 at three levels: -1, 0 and 1 as shown in table 2. According to the following transformation, the independent variables values (X_1, X_2 and X_3) were coded:

$$Zi = \frac{Xi - Xi0}{Xi} \quad \text{..... (Eq. 2)}$$

where Z*i* is the *i*th independent variable coded value, Xi is the *i*th independent variable uncoded value, X*i*^{0} is the *i*th independent variable uncoded value at its center point and Δ X*i* is the step change value. Multiple regression analysis was employed for the BBD matrix obtained responses and the second-order polynomial function result was used to correlate the independent variables and the response.

The McDA was applied to the output data through desirability function in order to find the optimal conditions for production of LD-CSNPs in regard to both PS and EE responses and hence they were transformed into an appropriate desirability scale. By combining the calculating individual desirabilities for each response, a composite of the multiresponse system will result, the geometric average of the individual desirabilities. A number of check-point experiments were carried out in the optimal area of the BBD in order to verify the optimization procedure validation, as predicted by desirability analysis and by comparing the experimental and predicted response.

Statistical Analysis: Minitab 15 (Minitab Inc, State College, PA) was employed for experimental design, regression analysis and McDA calculations. Analysis of variance (ANOVA) was the mean to test the independent variables and their interactions significancy and *p* value of 0.05 was used in all analyses. Student's *t* test was used to investigate the standardized effects of the independent variables and their interactions on the dependent variable. For comparing different fabrication conditions, statistical indices such as *t* value, *p* value, *F* value, correlation coefficient (*R*), determination coefficient (R^2) and adjusted determination coefficient (adj R^2) were used to assess the quadratic models and desirability composite values significancy.

Scanning Electron Microscopy (SEM): L-dopa (LD), unloaded and loaded optimized NPs (i.e.; o-CSNPs & o-LD-CSNPs) morphological characterizations (shape and structure) were examined using scanning electron microscope (AIS2300C, Angstrom-USA). The NPs were sprayed over carbon tape to be dried under vacuum and observed at an acceleration voltage of 20 kV.

Fourier Transform Infrared Spectroscopy (FTIR): For detecting any physicochemical interaction between the drug and the carrier, the (FTIR-600 FTIR Spectrometer, Main FTOS Biotech Engineering Management Co. Ltd-UK) was employed for LD, o-CSNPs and o-LD-CSNPs/KBr discs scanning at a resolution of 4 cm $^{-1}$, from 400 to 4000 cm $^{-1}$.

X-Ray Powder Diffraction (XRPD): At ambient conditions the (XRD-6000, Shimadzu-Japan) was employed for obtaining x-ray powder diffraction patterns of LD, o-CSNPs and o-LD-CSNPs. Operated at a voltage of 40 kV and 30 mA current,

samples were analyzed in the 2θ angle range of 5°–70°, scan step size of 0.02° (2θ) and time of 0.5 degree/min.

In Vitro Dissolution and Release Kinetic: Dialysis method was employed, a dialysis membrane–70 (Himedia-India) cut into equal pieces and pre–treated with phosphate buffer pH 7.4. Nanoparticles weight of 50 mg were placed in the dialysis bag and sealed at the both ends. Then bag was dipped into the dissolution medium of phosphate buffer pH 7.4 (receptor compartment), stirred at 100 rpm, maintained at 37 ^{0}C and closed to prevent evaporation. The withdrawn samples at regular time intervals were replaced with the same volume of fresh dissolution medium and measured spectrophotometrically using (SPECORD® 40-Analytik Jena AG-Germany) at 280 nm for LD against dummy nanoparticles as blank [14]. The release data were fitted according to five kinetic model-dependent equations in order to find the one with the best fit using DDSolver software (Zhang, China) [15]:

$$R = k_0 t \quad \text{..... (Eq. 3)}$$

$$\text{Log UR} = \frac{K1\ t}{2.303} \quad \text{..... (Eq. 4)}$$

$$R = k_H \sqrt{t} \quad \text{..... (Eq. 5)}$$

$$(UR)^{1/3} = k_{HC} t \quad \text{..... (Eq. 6)}$$

$$\text{Log } R = \text{Log } k_{KP} + n \text{ Log } t \quad \text{..... (Eq. 7)}$$

where R and UR are the released and unreleased percentages, respectively, at time (t): k_0, k_1, k_H, k_{HC} and k_{KP} are the rate constant of zero–order, first–order, Higuchi matrix, Hixson–Crowell and Korsmeyer–Peppas model respectively. Furthermore; Weibull dissolution model equation below can be successfully applied to almost all kinds of dissolution curves [16]. It expresses the accumulated fraction of the drug, Q, in solution at time, t, by:

$$Q = 1 - \exp\left[\frac{-(t-Ti)b}{a}\right] \quad \text{..... (Eq. 8)}$$

where: a is the scale parameter that defines process timescale, Ti is the lag time before the onset of dissolution or release process and will be zero in most cases and b is the shape parameter that characterizes the curve as either exponential when b=1 (case 1), sigmoid/S-shaped/with upward curvature followed by a turning point when b>1 (case 2) or parabolic/with a higher initial slope and after that consistent with the exponential when b<1 (case 3). Therefore; the properly selected optimized formula was further fitted into Weibull dissolution model equation.

RESULTS AND DISCUSSIONS

Model Fitting: The measured independent variables occur with large variations range from 243.9 nm to 513.1 nm for PS and from 07.21% to 60.80% for EE, indicate that NPs PS and EE were largely influenced by the selected variables. To the output data, multiple regression analysis was employed and the following second-order coded polynomial equations were established:

$$Y_1 = 291.42 + 35.39X_1 + 19.06X_2 + 8.08X_3 + 52.16X_1^2 + 52.49X_2^2 - 45.01X^2_3 + 40.99X_1X_2 - 17.74X_1X_3 - 19.74X_2X_3 \quad \text{..... (Eq. 9)}$$

$$Y_2 = 9.48 - 0.012X_1 - 7.9X_2 - 17.53X_3 + 9.23X_1^2 + 3.32X_2^2 + 13.30X^2_3 + 3.64X_1X_2 - 3.61X_1X_3 + 1.96X_2X_3 \quad \text{..... (Eq. 10)}$$

where Y_1 is the NPs size, Y_2 is the NPs EE and X_1, X_2 and X_3 are the CS concentration, CS/TPP mass ratio and LD/CS mass ratio respectively. X_1X_2, X_1X_3 and X_2X_3 are the interaction terms that show how the response changes when two variables are concurrently changed, while the effect of changes in each single variable on the response is reflected by X_1, X_2 and X_3 the main effect terms and X_1^2, X_2^2 and X_3^2 the quadratic terms. Table 3 presents the results of which the ANOVA was conducted to test the quadratic models significance and the lack of fit for the experimental data.

Fischer's ratio (F) confirm the models significancy, where F_{Y1} = 7.99 (p value = 0.017 < 0.05) and F_{Y2} = 9.61 (p value = 0.011 < 0.05). Model lack of fitness checked by the determination coefficient, where R^2_{Y1} = 0.935 and R^2_{Y2} = 0.945. Adjusted determination coefficient was adj R^2_{Y1} = 0.818 and adj R^2_{Y2} = 0.847.

Figure 1 depictes parity plots that demonstrate the high correlation coefficient values, i.e. R^2_{Y1} = 0.935 and R^2_{Y2} = 0.945 between the model prediction and actual responses by the quadratic models, figure 2 illustrates the normal probability plots where the error variances are homogenous, normally distributed and independent of each other and figure 3 shows plots of random residuales distribution without any trend, indicates good maximum response prediction with constant variance. Hence, these data confirm quadratic models reliability.

Student's *t*-test determines the significant of different and compares the standarized effects of

the model components and the results of which are demonstrated in table 4. Figures 4-7 illustrate constructions of three-dementional response surface graphs and two-dimentional contour plots of independent variables interactive effects on the responses. Based on equation 9, figures 4 and 5 show the response surface plots and their corresponding contour plots for PS. Based on equation 10, the response surface graphs and contour plots for EE are shown. Solving equations 9 and 10, optimum conditions for CSNPs production can be achieved for different values of independent variables within the experimental range, followed by McDA and desirability calculation. The optimum conditions are to be CS concentration of 1.2-1.6 mg/ml, CS/TPP mass ratio of 6-7 and LD/TPP mass ratio of 1.8-2. At these conditions, CSNPs ranging from 243-266 nm and EE ranging from 53-58% could be produced. Table 5 validates the optimization through a check point analysis in the optimal range. An accuracy of the predicted optimum conditions comes from the small errors of 3-5% which indicate that the observed responses are closed to the predicted.

Model Discussions: By employing RSM through BBD, the PS and EE responses influenced by CS concentration, CS/TPP mass ratio and LD/CS mass ratio factors were investigated. The NPs PS and EE are two properties important kinetically and dynamically to be optimized in order to improve drug loaded outcomes. Table 3, ANOVA revealed that both quadratic models are significant as evident by Fischer's *F* test, good fit and a significant amount of variation in the dependent variables can be explained. The *F* ratio and the corresponding *p* value indicate the possibility of explanation a significant amount of variation in the dependent variables, F_{Y1} = 7.99, p_{Y1} = 0.017 and F_{Y2} = 9.61, p_{Y2} = 0.011. Each model goodness of fit is evident from the determination coefficient, R^2_{Y1} = 0.935 and R^2_{Y2} = 0.945, which indicate that up to 93.5% and 94.5% of the response variability can be explained by these models, whereas the remaining 6.5% and 5.5% of the total response variations unexplained, respectively. The adjusted determination coefficient, adj R^2_{Y1} = 0.818 and adj R^2_{Y2} = 0.847 was also high and hence further confirms the models higher significancy. Good correlations between the observed and predicted responses by the models were confirmed by their high correlation coefficient values as visualized by the figure 1, parity plots, figure 2, normal probability of residuals plots and figure 3, residuals plots further confirmed the reliability and adequacy of the quadratic models, which demonstrate normal residuals distribution in both models.

Component's standarized effect measured by the *t* value for each component, thus higher *t* value and smaller corresponding *p* value the more significant the model component. Model Y_1, the quadratic effects of CS concentration and CS/TPP mass ratio, X^2_1 and X^2_2 with the highest *t* values of 4.08 and 4.05 respectively and the same smallest *p* value of 0.013 each, indicate both factors had a positive incremental effect on the PS. The LD/CS mass ratio quadratic effect, CS concentration and the interaction between CS concentration and CS/TPP mass ratio also had significant effects on the PS evidentially from their *t* and *p* values. The LD/CS mass ratio had the main effect among all of the model components and demonstarted the lowest effect on the response with *t* = 0.925 and *p* = 0.429. In contrast, model Y_2 the LD/CS mass ratio main and quadratic effect were the most significant components, where *t* = -7.77, *p* = 0.000 and *t* = 4.01, *p* = 0.016 respectively, which oppose each other by their opposite signs. Thus, the EE is not absolutely affected by and depends on this variable level. The CS/TPP mass ratio and CS concentration interaction contribute minor to the NPs EE, where *t* = 0.614, *p* = 0.597 and *t* = -3.51, *p* = 0.025 respectively.

By constructing three-dimensional response surface graphs and two-dimensional contour plots; figures 4-7, which are derived from equations 9 and 10, a better understanding of the independent variables and their interactions effects on the response and the conditions yielding the optimum values of both responses. Each graph at its central level one variable is kept constant, whereas the other two variables levels are varying within the experimental range. All three-dimensional response surfaces and their corresponding contour plots nonlinear nature demonstrates that there were considerable interactions between the independent variables, i.e. mutually dependent influences on the response.

The PS at the constant LD/CS mass ratio of 6 is shown in figure 4 A. By increasing the CS/TPP mass ratio at a certain CS concentration, results in a primary response decrease followed by an increment up to a maximal level and vs. The asymmetrical graph indicates that the extent of variations in response caused by alterations in CS concentration and CS/TPP mass ratio is not the same at different levels of the two variables. At higher CS concentration and CS/TPP mass ratio, the greatest PSs are obtained, while the reverse at lower levels. The contour plot, figure 5 A, showing a curvilinear plot, indicating a strong interaction between CS concentration and CS/TPP mass ratio. This plot, one can clearly observed that for each CS concentration and within a certain range of CS/TPP mass ratio a small NPs obtained, while alternating the CS/TPP mass ratio has a detrimental effect on the PS. Then, at the constant LD/CS mass ratio of

6, PS less than 300 nm cannot be gained at CS concentrations larger than 2.4, whatever the CS/TPP mass ratio was.

The PS at the constant CS/TPP mass ratio of 9 is shown in figure 4 B. The more complicated interaction between the CS concentration and LD/CS mass ratio results in a graph with asymmetrical and distorted nature, indicating unequal variations in response at different levels of variables, with a more intense interactive at higher CS concentrations. By increasing LD/CS mass ratio at each certain CS concentration, results in an initial increase up to a maximum level followed by a small reduction in size, while the reverse results in opposite effect on the PS. This graph shows that the smallest PSs obtained will be at lower CS concentrations and LD/CS mass ratios. The contour plot, figure 5 B, showing a nonlinear plot, with two separate zones of minimum PS, indicating that for each CS concentration range there are two LD/CS mass ratio ranges, which give rise to NPs with small sizes, while between these two zones, changing the LD/CS ratio in either direction has an increasing effect on the PS. This plot shows that NPs less than 300 nm cannot be achieved at constant CS/TPP mass ratio of 9 and CS concentrations larger than 2.8 mg/ml, whatever the LD/CS mass ratio was.

The PS at the fixed CS concentration of 2 mg/ml is shown in figure 4 C. The strong and complex interactions between the two variables, results in a nonlinear graph with distorted shape and seems to be more intense at either ends of the CS/TPP mass ratio experimental range. This graph shows that minimum PSs can be gained at lower CS/TPP and LD/CS mass ratios levels. The contour plot, figure 5 C, again as above distinct zones of minimum PS are observed, indicating for each range of CS/TPP mass ratio, two different ranges of LD/CS mass ratio at which NPs with minimum size could be obtained.

As it could be notice in figure 6 A, at the constant LD/CS mass ratio of 6, increasing CS concentration at a certain CS/TPP mass ratio, results in EE reduction down to a minimal level, with a subsequent increase of response at CS concentrations above 2 mg/ml and the same effect on the response by increasing the CS/TPP mass ratio at each certain CS concentration. Thus, the highest amounts of EE could be achieved at low CS concentrations with low CS/TPP mass ratios. The contour plot, figure 7 A, is a curvilinear plot where the two variables showing a strong interaction. This plots shows that EE values higher than 20% can be reached at constant LD/CS mass ratio of 6, CS concentrations less than 1.25 mg/ml and CS/TPP mass ratios less than 7.

The EE at the constant CS/TPP mass ratio of 9 is shown in figure 6 B. By increasing the LD/CS mass ratio at each certain CS concentration, the graph demonstrate an EE reduction down to a minimum, followed by a slight increment at LD/CS mass ratios higher than 8 and the same effect on the response by increasing the CS concentration at a certain LD/CS mass ratio which is more intense when the latter is less than 4 and when the former is more than 2 mg/ml. The contour plot, figure 7 B, due to strong interaction between the two variables will show a curvilinear nature. This plot shows that EE values larger than 30% can be reached at LD/CS mass ratios less than 3 at CS concentrations less than 1.4 mg/ml or more than 2.4 mg/ml.

The EE at the constant CS concentration of 2 mg/ml is shown in figure 6 C, which demonstrates a sharp decline in EE with an increment in LD/CS mass ratio from 2 to 8 at each certain CS/TPP mass ratio, while increasing the LD/CS mass ratio 8 to 9 has no influence on the EE. No considerable effect on the EE will take place upon changing the CS/TPP mass ratio at each certain LD/CS mass ratio. This graph shows that at constant CS concentration of 2 mg/ml the highest EE % can be reached within the experimental range of CS/TPP mass ratio at LD/CS mass ratio less than 3. The contour plot, figure 7 C, shows the highest EE % can be reached at LD/CS mass ratios less than 3 and CS/TPP mass ratios less than 9.

By combining all the response surface graphs and contour plots, a deduction that the smallest PS and maximum EE % can be produced from at low CS concentrations, low CS/TPP mass ratios and low LD/CS mass ratios, while the reverse has no effect on the both responses, but the effects extent is not the same and varied according to the different variable levels combinations.

It was found that the optimum conditions for production of CSNPs within minimum PS and maximum EE %, low CS concentration range of 1.2-1.6 mg/ml, low CS/TPP mass ratio of 6-7 and low LD/CS mass ratio of 1.8-2. By employing the checkpoint analysis, a confirmation that these conditions will result in NPs with PSs range from 243-266 nm and EE % range from 53-58 % can be obtained.

Scanning Electron Microscopy (SEM): The LD crystalline non-hygroscopic nature revealed by figure 8 A [17], figure 8 B shows that o-CSNPs have a tendency to coalesce results in irregularly shaped clumps due to the lower mass ratios and pH

which play a role affecting the particles size and porosity [18] and figure 8 C shows the roughly surfaced o-LD-CSNPs.

Fourier Transform Infrared Spectroscopy (FTIR): The LD characteristic FTIR peaks in figure 9 A are primary amine N-H bending vibration at 1520 cm^{-1} and aromatic O-H streching at 3200-3500 cm^{-1} [19], figure 9 B shows that o-CSNPs characteristic FTIR peaks are 3421 cm^{-1} becomes wider due to the H-bonding is enhanced and -NH_2 bending vibration shifts from 1610 cm^{-1} to 1572 cm^{-1} attributed to the linkage between TPP phosphoric groups and CS ammonium groups [20] and figure 9 C shows that o-LD-CSNPs characteristic LD FTIR peaks are 1275 cm^{-1}, 1568 cm^{-1} and 1651 cm^{-1} still appear which indicate no physicochemical interaction exist between the drug and the carrier.

X-Ray Powder Diffraction (XRPD): The LD XRPD as shown in figure 10 A at 2- values are 8.06°, 16.04° and 24.52° [21], figure 10 B shows that o-CSNPs characteristic XRDP 2- value is around 21^0 [22] and figure 10 C shows that o-LD-CSNPs characteristic XRPD 2 value of 16.04° which represents LD XRPD peak.

In Vitro Dissolution and Release Kinetic: The cumulative percentage of LD released from o-LD-CSNPs is shown in figure 11; where the initial phase of drug release is rapid due to the burst effect followed by release through diffusion mechanism. Due to the CS hydrophilic nature which enhance water ingress and hence LD dissolution and release is escalated [23]. Table 6 revealed that Korsmeyer-Peppas model is the best fitted and the non-Fickian (anomalous) diffusion was the release mechanism due to the release exponent was ($n \geq 0.45$) [24]. Weibull 4 model was the data obtained best fitted as shown in equation 11:

$$F_t = F_{max} X [1 - e^{-(t - Ti)\, b/a}] \text{ …..(Eq. 11)}$$

The release kinetic data were; Fmax=84.89%, a=2.05, b=0.778, T_i=0.11 and R^2=0.996. Therefore; the overall LD release equation will be:

$$Ft = 0.8489 X [1 - e^{-(t - 0.11)0.778/0.205}] \text{ …..(Eq. 12)}$$

CONCLUSIONS

By employing multiple linear regression analysis to the Box-Behnken experimental design, the quadratic models obtained were significant and valuable for LD-CSNPs PS and EE prediction. These responses were strongly affected by the three independent variables (CS concentration, CS/TPP mass ratio and LD/CS mass ratio) nonlinear relationship and mutual dependent influence. The optimum conditions for producing LD-CSNPs of minimum PS and maximum EE are CS concentration of 1.2-1.6 mg/ml, CS/TPP mass ratio of 6-7 and LD/CS mass ratio of 1.8-2 which results in LD-CSNPs with PSs range between 243-266 nm and EE range between 53-58 %. Further characterizations by employing SEM, XRPD and FTIR reveal drug homogenous distribution within and no physicochemical interaction with the carrier. The in vitro dissolution data was best fitted with Korsmeyer-Peppas and Weibull 4 models.

ACKNOWLEDGMENTS

The author highly appreciates and gratitude the valuable assistance of Baghdad College of Pharmacy for permission to perform this study in the research laboratory and author thanks the State Company for Drug Industries and Medical Appliances (SDI) (Samarra / Iraq) for providing the gift sample of l-dopa.

Table no. 1: Box-Behnken design matrix of three independent variables, each of three levels and observed responses

Experiment #	X_1 (CS, mg/ml)	X_2 [CS/TPP mass]	X_3 [LD/CS mass]	Y_1 [PS, nm]	Y_2 [EE, %]
1	-1	-1	0	358.6	35.34
2	+1	-1	0	371.2	21.42
3	-1	+1	0	342.3	10.30
4	+1	+1	0	513.1	12.00
5	-1	0	-1	243.9	50.05
6	+1	0	-1	318.8	60.80
7	-1	0	+1	314.6	11.52
8	+1	0	+1	311.1	09.30
9	0	-1	-1	271.1	47.32
10	0	+1	-1	321.5	30.40
11	0	-1	+1	318.9	18.63
12	0	+1	+1	284.1	08.00
13	0	0	0	295.2	07.21
14	0	0	0	291.2	09.05
15	0	0	0	285.2	08.13

Table no. 2: Box-Behnken design independent and dependent variables

Independent Variables		Levels		
		Low (-1)	Middle (0)	High (+1)
CS Concentration (mg/ml)	X_1	1	2	3
CS/TPP Mass Ratio	X_2	6	10	15
LD/CS Mass Ratio	X_3	2	6	9
Dependent Variables		**Objectives**		
Entrapment Efficiency (EE %)	Y_1	Maximize		
Particle Size (nm)	Y_2	Minimize		

Table no. 3: Analysis of variance (ANOVA) for regression models Y_1 and Y_2

Source	Degree of Freedom		Sum of Squares		Mean Square (Adjusted)		Fischer's Ratio (F)		*p* Value	
	Y_1	Y_2	Y_1	Y_2	Y_1	Y_2	Y_1	Y_2	Y_1	Y_2
Regression	9	9	50520.64	4228.15	5613.4	469.79	7.99	9.61	0.017	0.011
Linear	3	3	13257.37	2939.74	4419.12	979.91	4.80	18.61	0.064	0.003
Square	3	3	27020.07	974.27	9006.69	324.76	14.44	9.28	0.007	0.022
Interaction	3	3	9619.77	121.56	3206.59	40.52	4.73	0.95	0.066	1.111
Residual Error	5	5	3511.01	244.56	702.2	48.91				
Total	14	14	54031.66	4472.7						

Table no. 4: Quadratic Y_1 and Y_2 models different components coefficients

Factor	Coefficient		*p* Value	
	Y_1	Y_2	Y_1	Y_2
Intercept	291.42	9.48	0.017	0.011
X_1	35.39	-0.012	0.013	0.996
X_2	19.06	-7.90	0.098	0.025
X_3	8.08	-17.53	0.429	0.000
X_1^2	52.16	9.23	0.013	0.052
X_2^2	52.49	3.32	0.013	0.411
X_3^2	-45.01	13.30	0.024	0.016
X_1X_2	40.99	3.64	0.027	0.344
X_1X_3	-17.74	-3.61	0.236	0.347
X_2X_3	-19.74	1.96	0.193	0.597

Table no. 5: Check-point analysis of selected optimum conditions with predicted and observed responses

Batch	X_1	X_2	X_3	Y_1			Y_2		
				Predicted	Observed	Error (%)	Predicted	Observed	Error (%)
1	1.5	6	2	258.454	266.207	2.999	55.685	57.912	3.999
2	1.2	7	2	255.384	242.615	4.999	55.050	52.820	4.051
3	1.6	6.4	1.8	241.395	251.051	4.000	55.988	57.667	2.998

Table no. 6: 0-LD-CSNPs release kinetic data

Zero-Order Model		First-Order Model		Higuchi-Matrix Model		Hixson-Crowell Model		Korsmeyer-Peppas Model		
R^2	K_0 (%h^{-1})	R^2	K_1 (h^{-1})	R^2	K_H (%$h^{-1/2}$)	R^2	K_{HC} (h^{-1})	R^2	n	K_{KP} (%h^{-n})
0.721	12.185	0.953	0.248	0.972	29.681	0.908	0.067	0.974	0.474	30.941

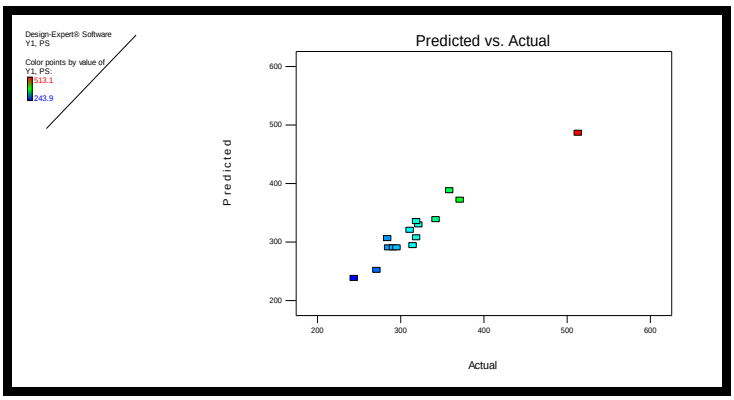

(A)

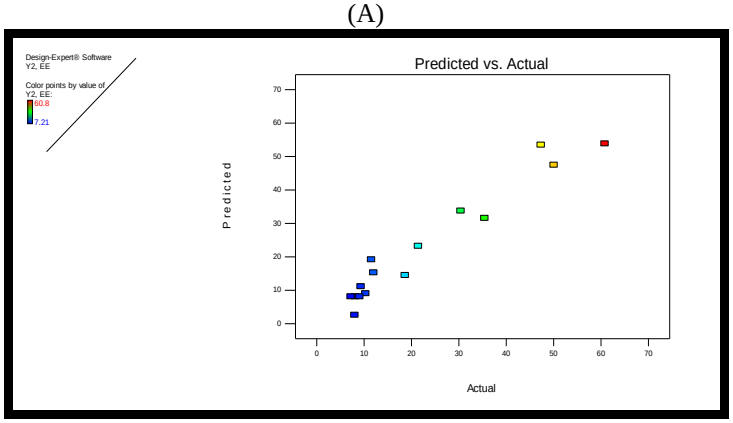

(B)

Fig. no. 1: Parity charts of predicted vs. observed responses for PS (A) and EE (B)

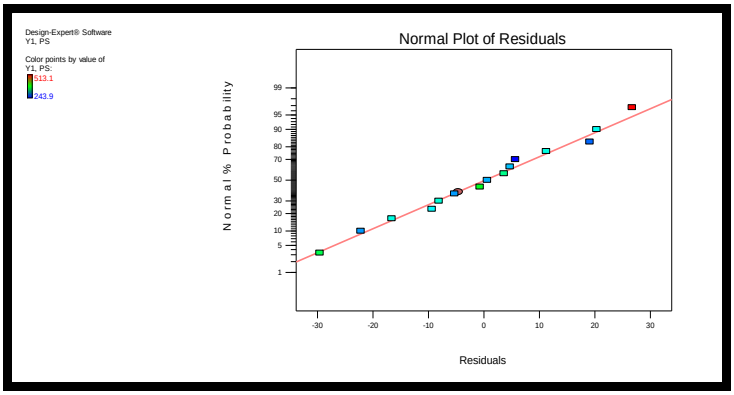

(A)

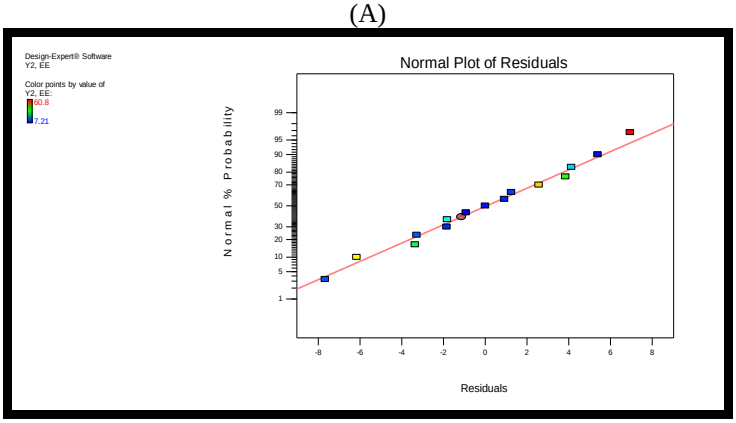

(B)

Fig. no. 2: Normal probability of residuals for PS (A) and EE (B)

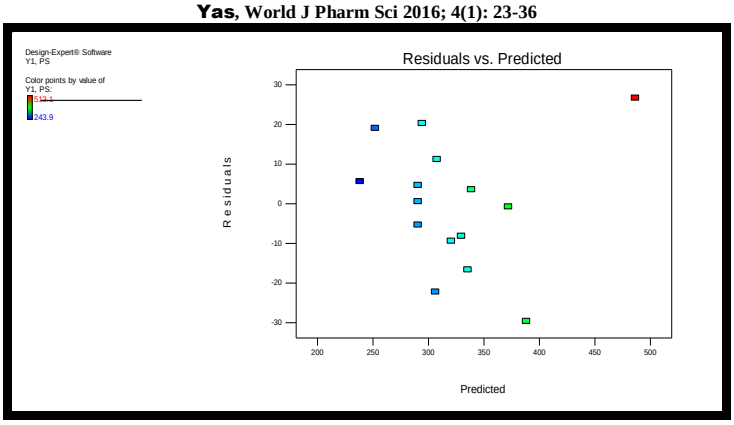

(A)

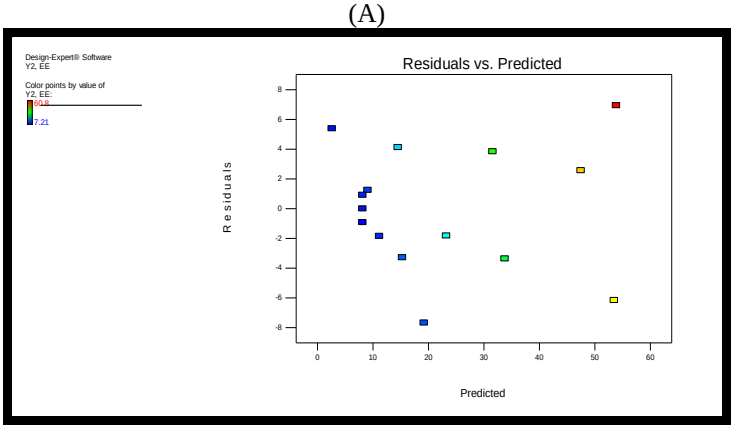

(B)

Fig. no. 3: Residual plot of PS (A) and EE (B)

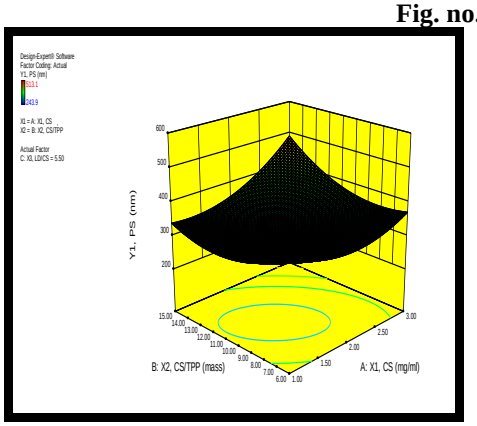

(A)

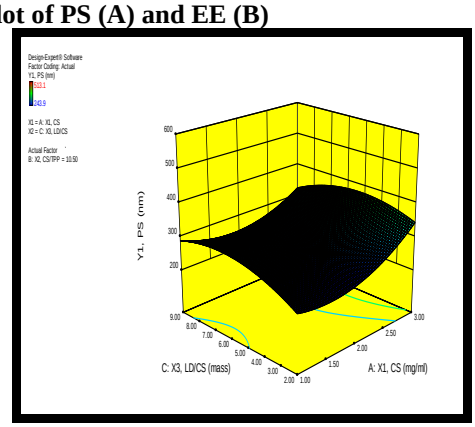

(B)

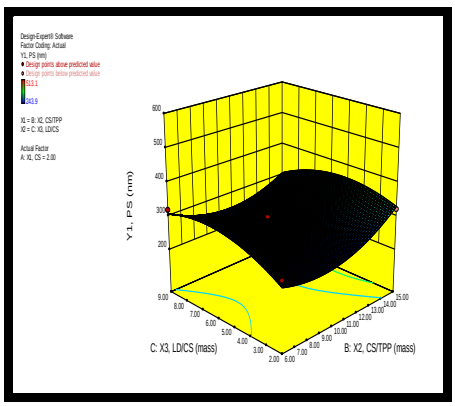

(C)

Fig. no. 4: Response surface graphs of PS at LD/CS mass ratio (A), CS/TPP mass ratio (B) and CS concentration (C)

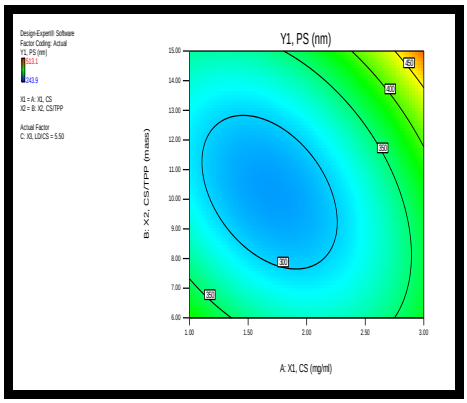

(A)

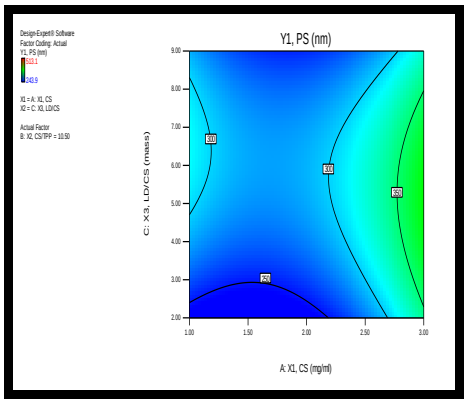

(B)

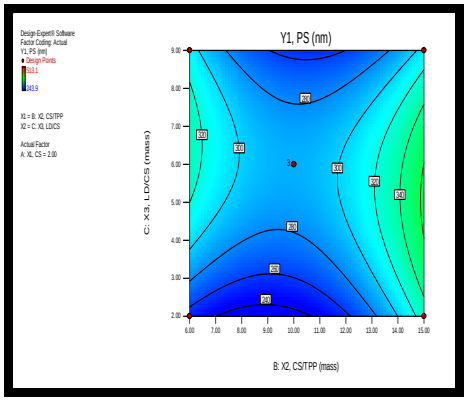

(C)

Fig. no. 5: Contour plots of PS at LD/CS mass ratio (A), CS/TPP mass ratio (B) and CS concentration (C)

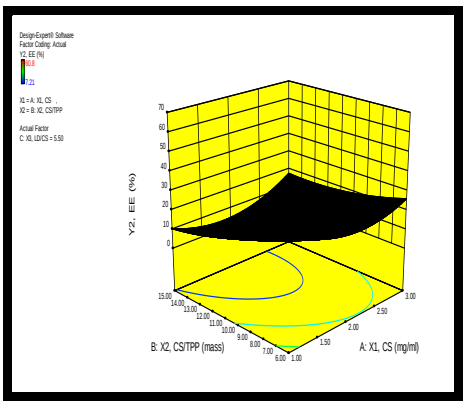

(A)

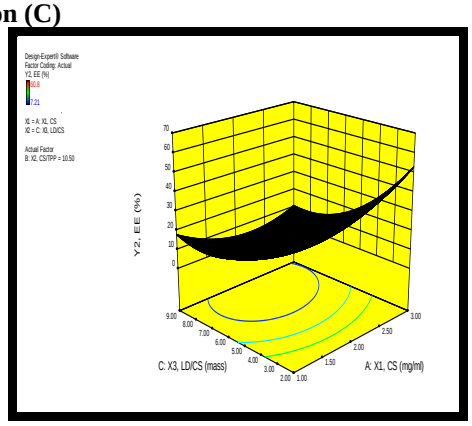

(B)

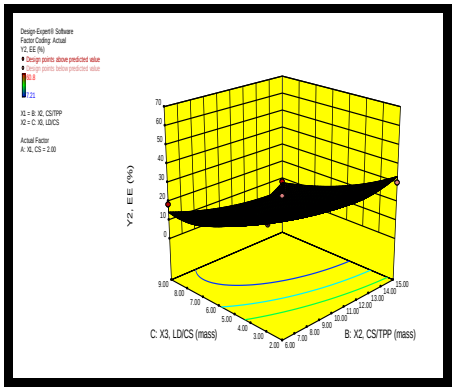

(C)

Fig. no. 6: Response surface graphs of EE at LD/CS mass ratio (A), CS/TPP mass ratio (B) and CS concentration (C)

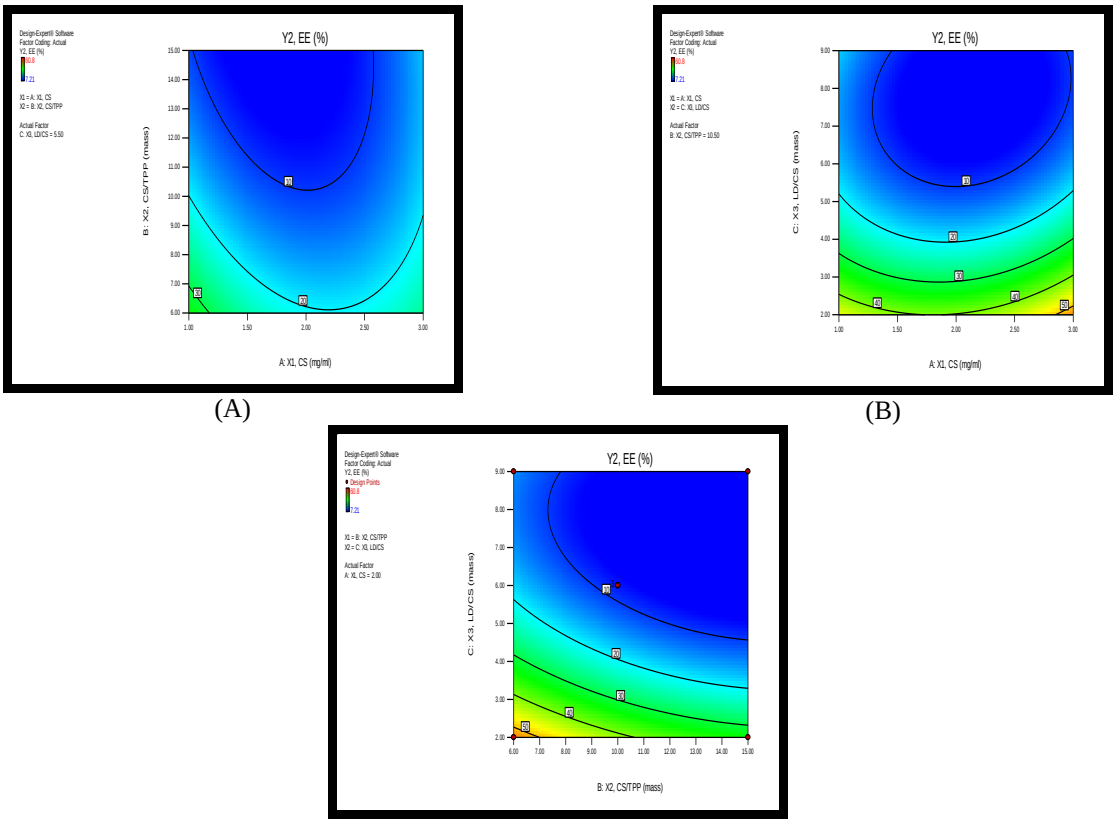

Fig. no. 7: Contour plots of PS at LD/CS mass ratio (A), CS/TPP mass ratio (B) and CS concentration (C)

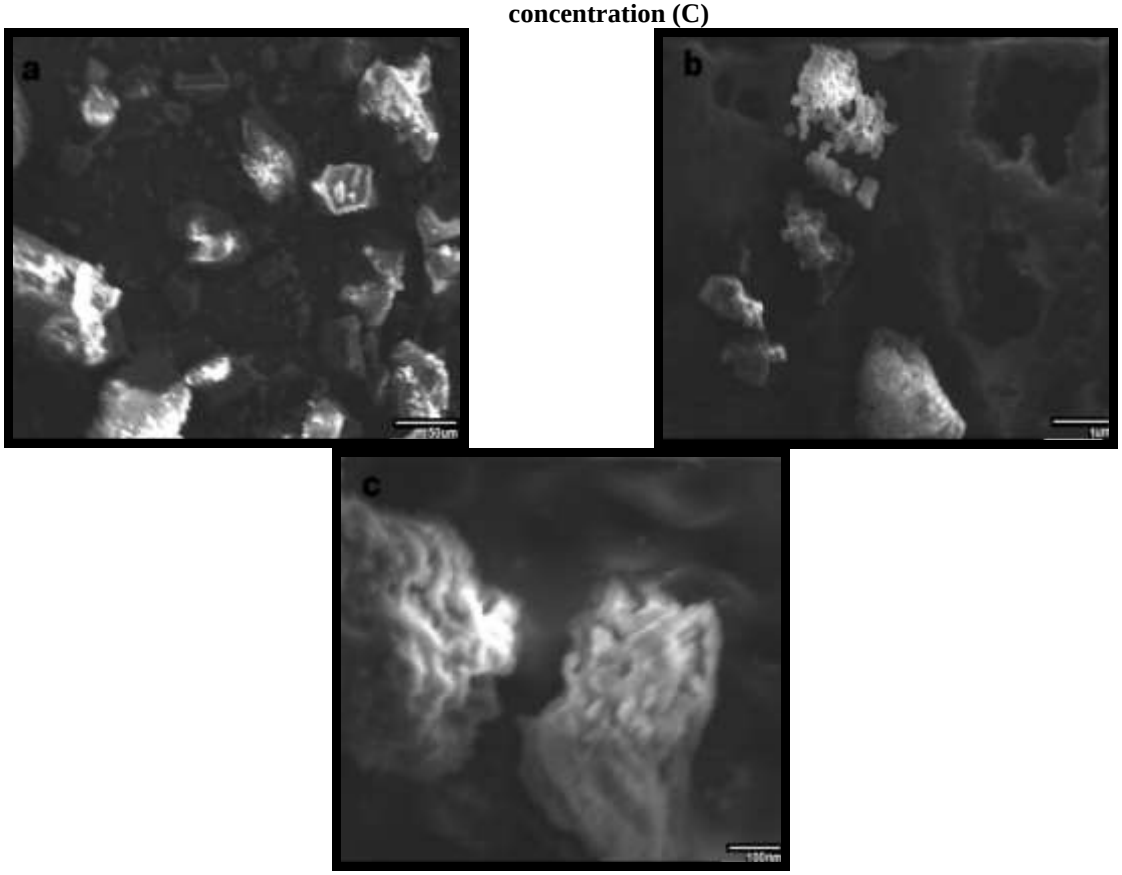

Fig. no. 8: SEM images of LD (A), o-CSNPs (B) and o-LD-CSNPs (C)

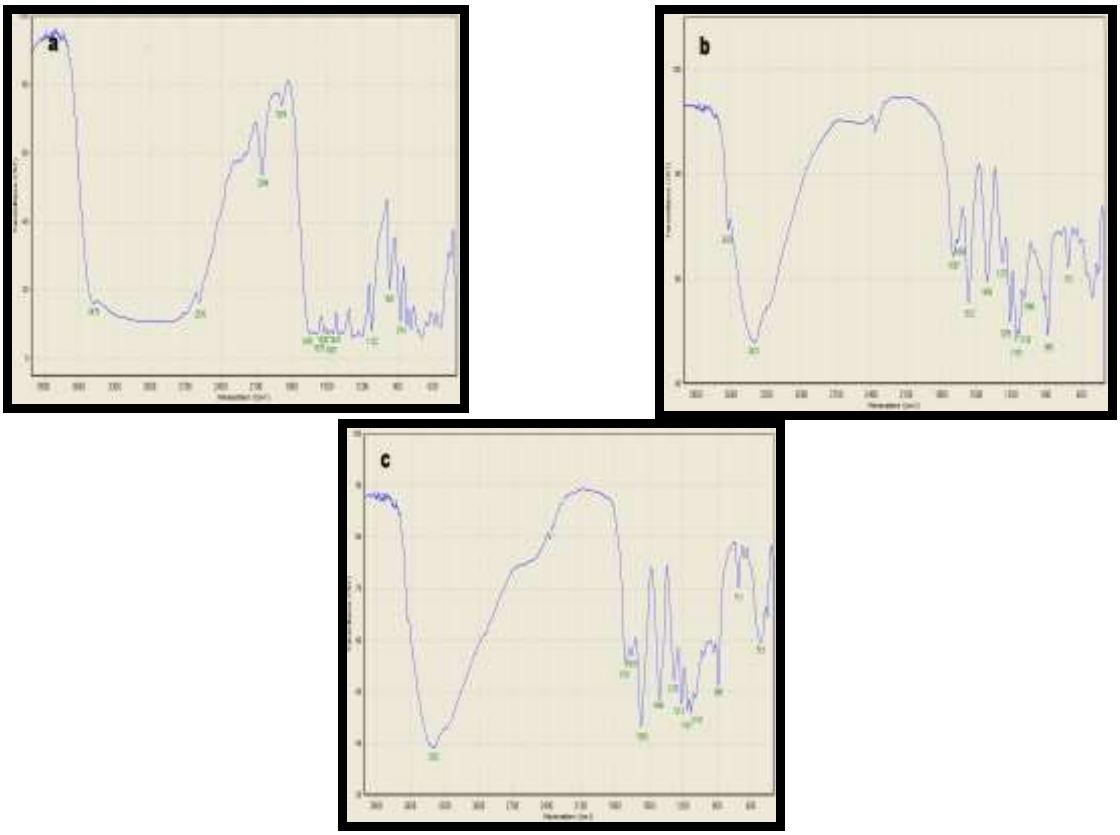

Fig. no. 9: FTIR spectra of LD (A), o-CSNPs (B) and o-LD-CSNPs (C)

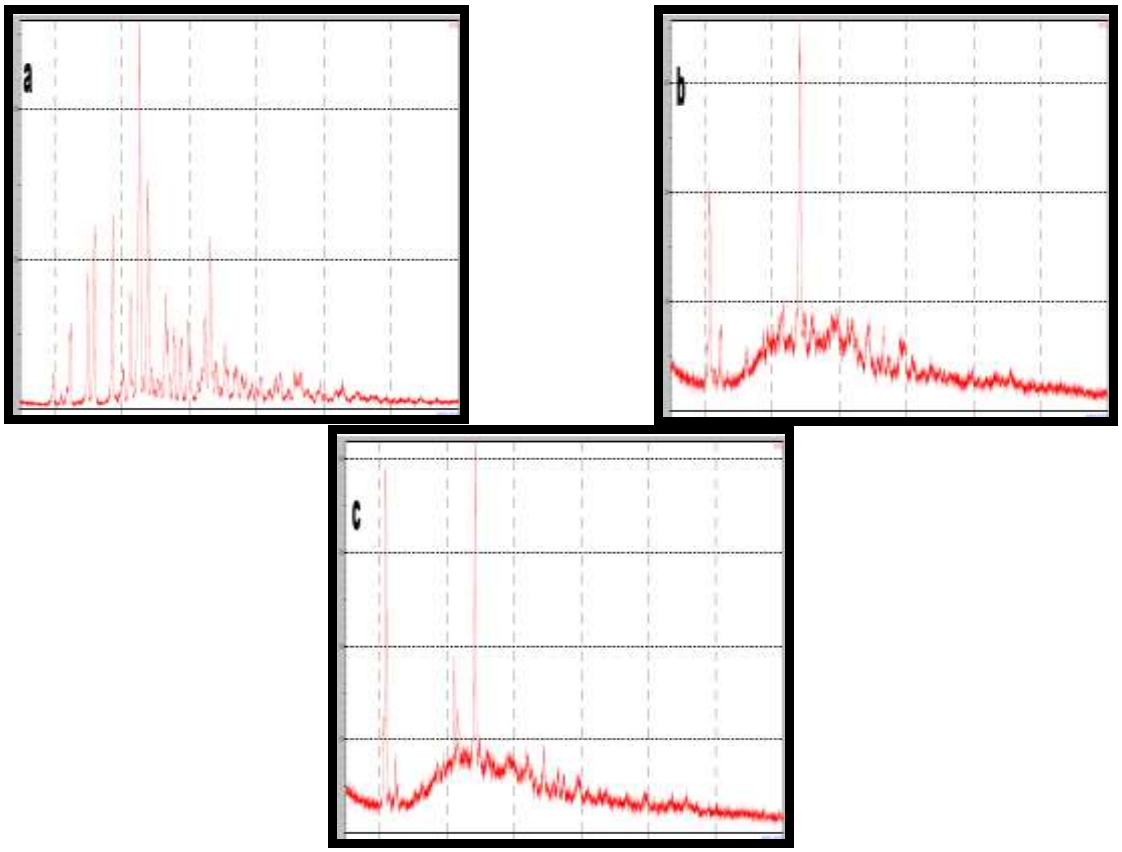

Fig. no. 10: XRPD of LD (A), o-CSNPs (B) and o-LD-CSNPs (C)

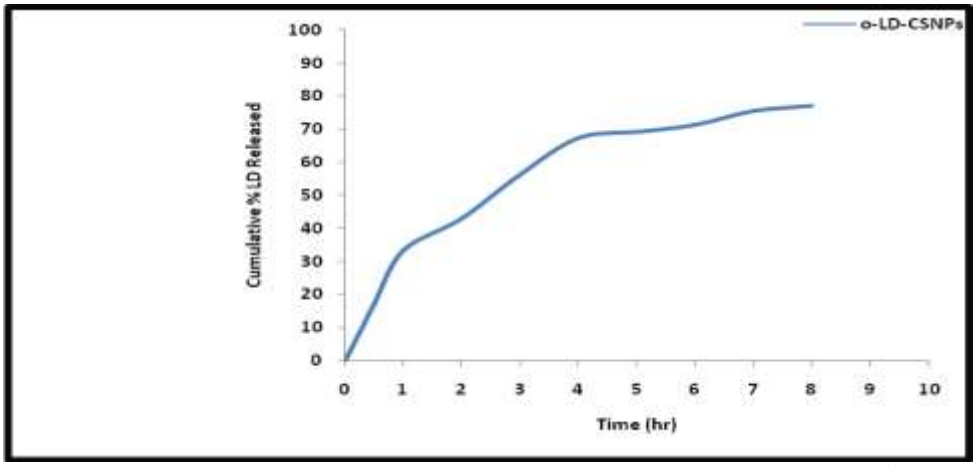

Fig. no. 11: Cumulative percentage of LD released from the o-LD-CSNPs in phosphate buffer of pH 7.4

REFERENCES

1. Dorsey ER, Constantinescu R, Thompson JP, Biglan KM, Holloway RG, Kieburtz K, Marshall FJ, Ravina BM, Schifitto G, Siderowf A, Tanner CM. Projected Number of People with Parkinson Disease in the Most Populous Nations, 2005 Through 2030. Neurology 2007; 68(5): 384 – 386.
2. Massano J, Bhatia KP. Clinical Approach to Parkinson 's disease: Features, Diagnosis, and Principles of Management. Cold Spring Harbor Perspectives in Medicine 2012; 2(6): 1 – 15.
3. Müller T. Drug Therapy in Patients with Parkinson's Disease. Translational Neurodegeneration 2012; 1(10): 1 – 13.
4. Abdel-Salam OME. Drug Therapy for Parkinson's Disease: An Update. World Journal of Pharmacology 2015; 4(1): 117 – 143.
5. Jenner P. Treatment of the Later Stages of Parkinson's Disease – Pharmacological Approaches Now and in the Future. Translational Neurodegeneration 2015; 4(3): 1 – 9.
6. Islam N, Rahman S. Pulmonary Drug Delivery: Implication for New Strategy for Pharmacotherapy for Neurodegenerative Disorders. Drug Discoveries & Therapeutics 2008; 2(5): 264 – 276.
7. Junise V. Sarawathi R. Development and Characterization of Chitosan Nanoparticles Loaded with Isoniazid. Journal of Pharmaceutical and Scientific Innovation 2015; 4(3): 190 – 195.
8. Georgieva D, Kostova B, Rachev D. Nanosized Polymeric Carriers for Dexamethasone Controlled Delivery. Journal of Chemical and Pharmaceutical Research 2015; 7(3): 1767 – 1772.
9. Eriksson L, Johansson E, Kettaneh-wold N, Wikström C, Wold S. Design of Experiments: Principles and Applications. Umea: Umetrics academy; 2008: 8–24.
10. Linkov I, Satterstrom FK, Kiker G, Batchelor C, Bridges T, Ferguson E. From Comparative Risk Assessment to Multicriteria Decision Analysis and Adaptive Management: Recent Developments and Applications. Environment International 2006; 32(8): 1072 – 1093.
11. Sadigh-Eteghad S, Talebi M, Farhoudi M, Mahmoudi J, Reyhani B. Effects of Levodopa Loaded Chitosan Nanoparticles on Cell Viability and Caspase-3 Expression in PC12 Neural Like Cells. Neuroscience 2013; 18(3): 281 – 283.
12. Gilani K, Moazeni E, Fazeli MR. Preparation and Characterization of Spray Dried Inhalable Powders Containing Chitosan Nanoparticles for Pulmonary Delivery of Isoniazid. Journal of Microencapsulation 2011; 28(7): 605 – 613.
13. Jayanudin, Rochmadi, Wiratni, Yulvianti M, Barleany DR, Ernayati W. Encapsulation Red Ginger Oleoresin (*Zingiber officinale* var. Rubrum) With Chitosan-alginate as Wall Material Using Spray Drying. Research Journal of Applied Sciences, Engineering and Technology 2015; 10(12): 1370 – 1378.
14. Junise V, Saraswathi R. Development and Characterization of Inhaled Chitosan Nanoparticles Loaded with Isoniazid. Journal of Pharmaceutical Technology, Research and Management 2014; 2(2): 159 – 170.
15. Zhang Y, Huo M, Zhou J, Zou A, Li W, Yao C, Xie S. DDSolver: An Add-In Program for Modeling and Comparison of Drug Dissolution Profiles. The AAPS Journal 2010; 12(3): 263–271.
16. Costa P, Lobo JMS. Modeling and Comparison of Dissolution Profiles. European Journal of Pharmaceutical Sciences. 2001; 13(2):123 – 133.
17. Luinstra M, Luinstra F, Hagedoorn P, Moes JR, Frijlink HW, de Boer AH. A Levodopa Dry Powder Inhaler for the Treatment of Parkinson's Disease Patients in off Periods. European Journal of Pharmaceutics and Biopharmaceutics 2015; 97: 22 – 29.
18. Martins AF, de Oliveira DM, Pereira AGB, Rubira AF, Muniz EC. Chitosan/TPP Microparticles Obtained by Microemulsion Method Applied in Controlled Release of Heparin. International Journal of Biological Macromolecules 2012; 51(5): 1127 – 1133.
19. Zhou YZ, Alany RG, Chuang V, Wen J. Optimization of PLGA Nanoparticles Formulation Containing L-DOPA by Applying the Central Composite Design. Drug Development and Industrial Pharmacy 2013; 39(2): 321 – 330.
20. Wu Y, Yang W, Wang C, Hu J, Fu S. Chitosan Nanoparticles as a Novel Delivery System for Ammonium Glycyrrhizinate. International Journal of Pharmaceutics 2005; 295(1-2): 235 – 245.
21. Kura AU, Al Ali SHH, Hussein MZ, Fakurazi S, Arulselvan P. Development of a Controlled-Release Anti-Parkinsonian Nanodelivery System using Levodopa as the Active Agent. International Journal of Nanomedicine 2013; 8: 1103 – 1110.
22. Zeng R, Tu M, Liu HW, Zhao JH, Zha ZG, Zhou CR. Preparation, Structure and Drug Release Behaviour of Chitosan-Based Nanofibres. The Institution of Engineering and Technology (IET) Nanobiotechnology 2009; 3(1): 8 – 13.
23. Kouchak M, Azarpanah A. Preparation and *In Vitro* Evaluation of Chitosan Nanoparticles Containing Diclofenac Using the Ion-Gelation Method. Jundishapur Journal of Natural Pharmaceutical Products 2015; 10(2) e23082: 1 – 7.
24. Chime SA, Onunkwo GC, Onyishi II. Kinetics and Mechanisms of Drug Release from Swellable and Non Swellable Matrices: A Review. Research Journal of Pharmaceutical, Biological and Chemical Sciences 2013; 4(2): 97 – 103.